Title

Operando Electrochemical Liquid-Cell Scanning Transmission Electron Microscopy (EC-STEM) Studies of Evolving Cu Nanocatalysts for CO2 Electroreduction

Journal

ACS Sustainable Chemistry & Engineering, 11(10)

ISSN

2168-0485

Authors

Yang, Yao
Shao, Yu-Tsun
Jin, Jianbo
et al.

Publication Date

2023-03-13

DOI

10.1021/acssuschemeng.2c06542

Peer reviewed

Operando Electrochemical Liquid-Cell STEM (EC-STEM) Studies of Evolving Cu Nanocatalysts for CO_2 Electroreduction

Yao Yang,[1,2,3,*] Yu-Tsun Shao,[4] Jianbo Jin,[1] Julian Feijóo,[1,3] Inwhan Roh,[1,3] Sheena Louisia,[1,3] Sunmoon Yu,[3,5] Maria V. Fonseca Guzman,[1,3] Chubai Chen,[1,3] David A. Muller,[4,6] Héctor D. Abruña,[6,7,*] Peidong Yang[1,3,5,8,*]

[1]Department of Chemistry, University of California, Berkeley, CA 94720, USA.
[2]Miller Institute for Basic Research in Science, University of California, Berkeley, CA 94720, USA.
[3]Chemical Sciences Division, Lawrence Berkeley National Laboratory, Berkeley, CA 94720, USA.
[4]School of Applied and Engineering Physics, Cornell University, Ithaca, NY 14853, USA.
[5]Department of Materials Science and Engineering, University of California, Berkeley, CA 94720, USA.
[6]Kavli Institute at Cornell for Nanoscale Science, Cornell University, Ithaca, NY 14853, USA.
[7]Department of Chemistry and Chemical Biology, Cornell University, Ithaca, NY 14853, USA.
[8]Kavli Energy NanoScience Institute, Berkeley, CA 94720, USA.
*Corresponding authors: yaoyang1@berkeley.edu, hda1@cornell.edu, p_yang@berkeley.edu

Abstract:
The design and synthesis of nanocatalysts with well-defined sizes, compositions and structures have revolutionized our accessibility to tunable catalyst activity and selectivity for a variety of energy-related electrochemical reactions. Nonetheless, establishing structure-(re)activity correlations requires the understanding of the dynamic evolution of pristine nanocatalysts and the identification of their active states under operating conditions. We previously communicated the *operando* observation of Cu nanocatalysts evolving into active metallic Cu nanograins for CO_2 electroreduction (*Nature*, 2022).[1] Here, we expand our discussion to the technical capabilities and further research applications of *operando* electrochemical liquid-cell scanning transmission electron microscopy (EC-STEM), which enables quantitative electrochemistry while tracking dynamic structural evolution of sub-10 nm Cu nanocatalysts. The co-existent H_2 bubbles, often disruptive to *operando* spectroscopy, are an effective approach to create a thin-liquid layer that significantly improves spatial resolution while remaining electrochemically accessible to Cu nanocatalysts. *Operando* four-dimensional (4D) STEM in liquids provides insights into the complex structure of active polycrystalline metallic Cu nanograins. With continuous technical developments, we anticipate that *operando* EC-STEM will evolve into a powerful electroanalytical method to advance our understanding of a variety of nanoscale electrocatalysts at solid/liquid interfaces.

Keywords: *Operando*; EC-STEM; 4D-STEM; CO_2RR; Dynamic Evolution; Cu nanocatalysts

Introduction:

Electrocatalysis is the cornerstone of sustainable electrochemical energy technologies with the potential to significantly mitigate the environmental impacts of fossil fuels. Although conventional *ex situ* characterizations provide a baseline understanding, many nanoscale electrocatalysts undergo significant structural transformation under electrochemical reactions, which calls for the use of *operando*/*in situ* methods.[1-7] In particular, the dynamic evolution of

highly active Cu nanocatalysts under CO_2 reduction reaction (CO_2RR) conditions requires nanoscale time-resolved analytical techniques.[8] Cu nanocatalysts (sub-10 nm) were previously reported to selectively convert CO_2 to multicarbon (C_{2+}) products at lower overpotentials (-0.8 vs. reversible hydrogen electrode, RHE), than bulk Cu counterparts.[9] In our recent work, a suite of *operando* electron microscopy and X-ray methods were employed to identify the structure of the active sites in Cu nanocatalysts as "Cu nanograins".[1] At CO_2RR operating potentials, the hydrogen evolution reaction (HER) accounts for a significant fraction of the Faradaic efficiency. The H_2 bubbles, generated along with CO_2RR, often pose a significant challenge for *operando* vibrational spectroscopy and X-ray absorption spectroscopy that require a stable liquid thickness for background subtraction in spectroscopic analysis.[4] Electrochemical liquid-cell scanning transmission electron microscopy (EC-STEM) cells have a liquid thickness of 500 nm or thicker at different locations of the cell due to the bulging out of the SiN_x windows in order to adjust to the pressure difference between the liquid cell and the TEM chamber.[10] With such a thick liquid layer, the spatial resolution of STEM imaging in liquids is severely compromised, which makes it particularly challenging to resolve sub-10 nm features at a beam dose below the threshold of affecting electrochemical reactions.[11] The thick liquid also poses a formidable challenge to the use of electron diffraction for structural information in liquids.[12-14] Our previous studies introduced the "thin-liquid" strategy enabled by H_2 bubbles electrogenerated during cathodic corrosion, which enabled Four-dimensional (4D) STEM diffraction imaging in liquids.[15] In this *operando* EC-STEM study, we take advantage of the co-existent H_2 bubbles formed during CO_2RR to create a thin liquid layer, which significantly improves spatial resolution for resolving dynamic evolution at the nanoscale. Four-dimensional (4D) STEM diffraction imaging is readily accessible in thin liquid films to provide structural information on the polycrystalline metallic Cu nanograins. In the end, we identified several key aspects that are required to enable more quantitative electrochemistry in EC-STEM, so that this fast-growing technique can make significant contributions to the vast energy materials community, in general, and the electrocatalysis community, in particular.

Results & Discussion:

Operando EC-STEM enables quantitative electrochemistry and simultaneous tracking of the dynamic evolution of nanoscale electrocatalysts under operating conditions (Fig. 1a). The electrochemical liquid cell is composed of a liquid layer with a 500 nm spacer in between two silicon nitride (SiN_x) windows (each is about 50 nm thick).[16,17] The three-electrode system includes an electron-transparent and electrochemically inert glassy carbon working electrode (WE) with a thickness of ~50 nm and geometric area of ~2,500 μm^2 (Fig. 1b). The Pt counter electrode (CE) with a large area of 0.29 mm^2, relative to the WE, enables a rapid polarization in response to the applied potential on the WE. The circular CE can establish a symmetrical electrical field and uniform current density around the WE and is positioned sufficiently far away from the WE to minimize the effects of electrochemical reactions of the CE on the WE. Given

the sub-μm electrolyte, it is challenging to accommodate a standard RE such as Ag/AgCl in KCl solution with a salt bridge within the liquid cell. Pt serves as a pseudo-RE for its chemical stability, wide potential window, and facile nanofabrication.

A 7 nm Cu nanoparticle (NP ensemble was deposited on the glassy carbon WE for electrochemical measurements in CO_2-saturated 0.1 M $KHCO_3$. The as-synthesized NP ensemble rapidly oxidizes to Cu_2O after brief air exposure prior to electrochemical reactions.[1] The cyclic voltammetric (CV) profile of the 7 nm Cu NP ensemble shows well-defined reduction and oxidation peaks, corresponding to Cu_2O reduction to Cu and Cu reoxidation to Cu_2O, respectively (Fig. 2a). The electroreduction peak of the NP ensemble is located at ~0.35 V vs. RHE, which is consistent with the reduction peak of NP ensembles measured in a standard electrochemical H-cell at ~0.45 V vs. RHE (Fig. S1a). The discrepancy may come from the uncertainty in potential conversion given that the potential of the Pt pseudo reference electrode (pseudo-RE) is estimated be 0.8 ± 0.1 V vs. reversible hydrogen electrode (RHE).[1,4] The chronoamperometric (CA) profile of the Cu NP ensemble at 0 V vs. RHE simulates the operating condition near the hydrogen evolution reaction (HER) with a steady-state current of about -10 nA (Fig. 2b). The CA profile at -0.8 V vs. RHE simulates the optimal CO_2RR potential for C_{2+} formation on a 7 nm NP ensemble[9] and shows a stable current plateau of about -100 nA (about -4 mA/cm^2 by normalizing the current to the geometric area of the WE). This is within the same order of magnitude as the operating current density in a realistic electrochemical H-cell (about -14 mA/cm^2) at -0.8 V vs. RHE (Fig. S1b). The ohmic resistance was measured to be 20-30 kΩ in 0.1 M $KHCO_3$ electrolyte with electrochemical impedance spectroscopy (EIS). Given ~100 nA operating current in EC-STEM, the iR drop was estimated to be 2-3 mV, a negligible value when compared to the operating potential. In summary, these electrochemical measurements indicate that *operando* EC-STEM is capable of delivering a comparable reaction rate (current density) at a comparable driving force (applied potential; overpotential), relative to standard electrochemical measurements.

Operando EC-STEM under CO_2RR-relevant conditions makes use of the electrogenerated H_2 bubbles to generate a thin liquid layer with significantly enhanced spatial resolution. With linear sweep voltammetry (LSV) from 0.4 to around 0 V vs. RHE, H_2 gas bubbles are formed (Fig. S2). An initial potential below the open circuit potential (OCP) at about 0.6 V vs. RHE was chosen in order to start with a reducing current and avoid undesirable structural changes due to oxidation from Cu_2O to CuO at more positive potentials. As the LSV reaches around 0 V vs. RHE, the thick liquid layer is displaced, and dynamic particle aggregation is clearly resolved (Fig. S2c). In an effort to determine the thickness of the thin liquid layer, low-loss electron energy loss spectroscopy (EELS) was performed and analyzed based on Beer's law (Fig. S3).[10,18] The thickness of the dry SiN_x windows was measured to be about 100 nm, which is consistent with the combined thickness of two layers of 50 nm-thick SiN_x windows. The total thickness of the thin-liquid layer and the SiN_x windows was measured to be 200 ± 15 nm (Table S1). Thus, the

estimated thickness of the thin liquid layer is about 100 nm. Assuming that the liquid layer has the same thickness below and above the H_2 bubbles within the cell, the liquid covering the WE is about 50 nm thick. It should be noted that both CA profiles at 0 and -0.8 V vs. RHE were acquired after H_2 bubble formation (Fig. 2b). The stable current plateau with mA/cm^2-level current density at -0.8 V vs. RHE suggests that that the hydrophilic glassy carbon WE, covered with a thin-liquid layer, remains electrochemically accessible to CO_2RR instead of drying out after forming H_2 bubbles.

With electrochemical measurements and liquid thickness quantification established, *operando* EC-STEM imaging was performed to investigate the dynamic morphological changes of Cu NPs under CO_2RR relevant conditions. Fig. 3 provides an overview of the transformation of the 7 nm Cu NP ensemble under applied potentials. The high-angle annular dark-field detector (HAADF) STEM image shows that the as-synthesized 7 nm Cu NPs are monodisperse and self-assembled in a hexagonal packing on the carbon substrate (Fig. 3a). The interparticle distance was estimated to be ~1 nm based on our previous resonant soft X-ray scattering study.[19] After the LSV scan from 0.4 to 0 V vs. RHE, the *operando* EC-STEM image in Fig. 3b captures both the remaining 7 nm Cu NPs on the left and the initial aggregation into loosely connected Cu nanograins (Figs. S4, S5). No beam damage was observed at a low beam dose of ~50 e$^-$/nm^2 per image frame (dose rate of ~12.5 e$^-$/nm^{2}s).[9] Under CO_2RR relevant conditions (-0.8 V vs. RHE), those newly formed Cu nanograins undergo further aggregation/coalescence and reach a steady-state structure of closely packed Cu nanograins (50-100 nm, Figs.3, 4a). Detailed analysis of *operando* EC-STEM movies of dynamic evolution can be found in our recent work.[1]

With the thin-liquid strategy, this study can go beyond conventional STEM imaging and enable 4D-STEM diffraction imaging in liquids. The 4D-STEM dataset is captured on an electron microscopy pixel array detector (EMPAD) with single electron sensitivity and fast readout speed[20,21] which are crucial for low-dose electron diffraction in beam-sensitive liquids.[1,15] 4D-STEM diffraction imaging was acquired at an estimated beam dose of ~2,000 e$^-$/nm^2 (a dose rate of ~6 e$^-$/nm^{2}s). The HAADF-STEM image shows that irregular Cu nanograins (50-100 nm) are formed at -0.8 V vs. RHE under CO_2RR relevant conditions (Fig. 4a). A virtual bright-field (BF) STEM image was reconstructed by integrating the (000) transmitted spot of the 4D-STEM dataset which shows the granular features of those Cu nanograins (Fig. 4b). Two representative diffraction patterns were selected to show the different orientations of the Cu nanograins (Figs. 4c,d). Some regions of the Cu nanograins show a diffraction pattern with Cu{111} (2.1 Å) and Cu{200} (1.8 Å) spots near the Cu[110] zone axis (Fig. 4c). However, the vast majority of the Cu nanograins show highly polycrystalline diffraction patterns like the one in Fig. 4d. A false-color dark-field 4D-STEM composite image (Fig. 4e), extracted from three diffraction spots (1 (red), 2 (green) and 3 (blue)) in Fig. 4c, shows crystal domains matching crystal orientations of those three diffraction spots. The magnified composite image and corresponding virtual BF-

STEM image (Figs. 4f,g), as well as diffraction patterns in Figs. 4h,l, better illustrate that multiple Cu nanograins with different crystal orientations can exist within each particle.

In summary, this study illustrates the electrochemical capability of *operando* EC-STEM and presents the application of the "thin-liquid" strategy enabled by electrogenerated H_2 bubbles under CO_2RR conditions. The pristine 7 nm Cu NP ensemble undergoes a dramatic structural transformation into an active state of polycrystalline metallic Cu nanograins (50-100 nm). *Operando* electrochemical 4D-STEM structural analysis provides a glimpse into the complex nature of active metallic Cu nanograins under CO_2RR conditions. Future work on quantifying grain sizes and density may provide additional insights into how to tune the structure of Cu nanograins for more effective C-C coupling reactions. This study points out the need for *operando* methods to investigate active sites of electrocatalysts instead of relying on conventional *ex situ* methods, especially for highly reactive Cu nanocatalysts.[22-24] We would also like to point out several future directions that are required to make *operando* EC-STEM more accessible to the broad energy materials community.

(1) **Quantification of applied potentials**. A rigorous calibration of the potential of the Pt pseudo-RE in different electrolyte environments will be instrumental to benchmark electrochemistry in *operando* EC-STEM. The uncertainty of the Pt pseudo-RE potential values (~0.1 V) is less of an issue for electrochemical reactions such as CO_2RR, N_2 electroreduction or oxygen evolution reaction (OER) that require significantly large overpotentials to operate. However, a stable RE with an uncertainty below 10 mV will be required to study electrochemical reactions that are highly sensitive to small changes in overpotentials, in particular, hydrogen oxidation/evolution reactions (HOR/HER) and the oxygen reduction reaction (ORR) for fuel cells. In comparison, a commercial RE electrode, such as Ag/AgCl or Hg/HgO, can connect to the liquid cell externally and serve as a stable potential reference point with a stability of the order of 1 mV.[25,26] We anticipate that the incorporation of a more stable RE will be critical to enable more quantitative electrochemistry, so that EC-STEM can evolve into a reliable *operando* electrochemical technique, like *operando* X-ray absorption spectroscopy, that can be widely and readily used by electrochemists to investigate electrochemical reaction dynamics with unprecedented spatiotemporal resolutions.

(2) **Quantification of current density**. Preliminary comparison of the average current density on a glassy carbon WE in EC-STEM, and that in standard electrochemical cells, suggests that the reaction rates are on the same order of magnitude. The current density, normalized to the geometric area of the WE, only reveals limited information about intrinsic reaction rates. Quantification of the electrochemical surface area (ECSA) of electrocatalysts in EC-STEM will be critical to provide information on intrinsic activity per active sites and potential-dependent surface coverage of reaction intermediates. Modelling of the electric field distribution of the WE can advance our understanding of the reaction rate as a function of

applied potentials, electrolyte, adsorbates and types of substrates, among others.[27] In particular, the heterogeneity in electric field distributions may have a strong effect on the reaction kinetics in the particularly thin liquid layer.

(3) **Improvement of spatial resolution without forming bubbles**. How can we expand *operando* EC-STEM to electrochemical reactions that do not generate H_2 bubbles, such as HOR and ORR as well as in most battery applications?[28-30] There is a need to push the technical limit of nanofabrication for a pristine liquid layer thickness on the order of 100 nm and thinner SiN_x windows.

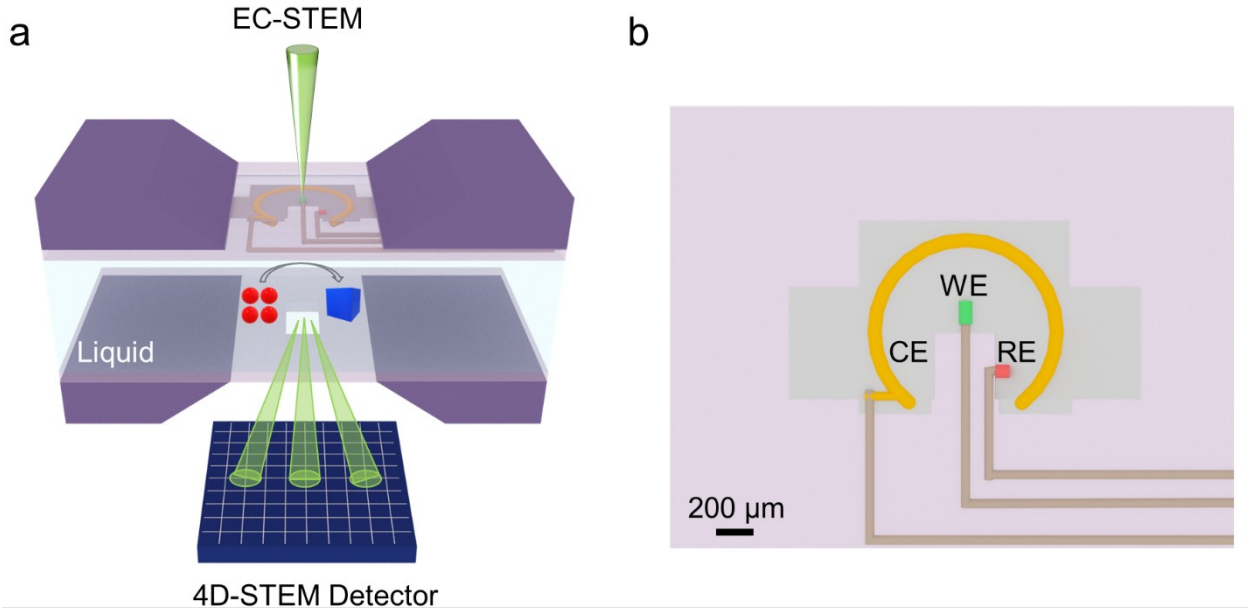

Figure 1. (a) Schematic of *Operando* EC-STEM with 4D-STEM detector that enables reliable electrochemistry while monitoring dynamic morphological and structural changes under electrocatalytically relevant conditions. (b) Schematic of the three-electrode system with nanocatalysts deposited on the working electrode (WE) and Pt counter and pseudo-reference electrodes (CE and pseudo-RE, respectively).

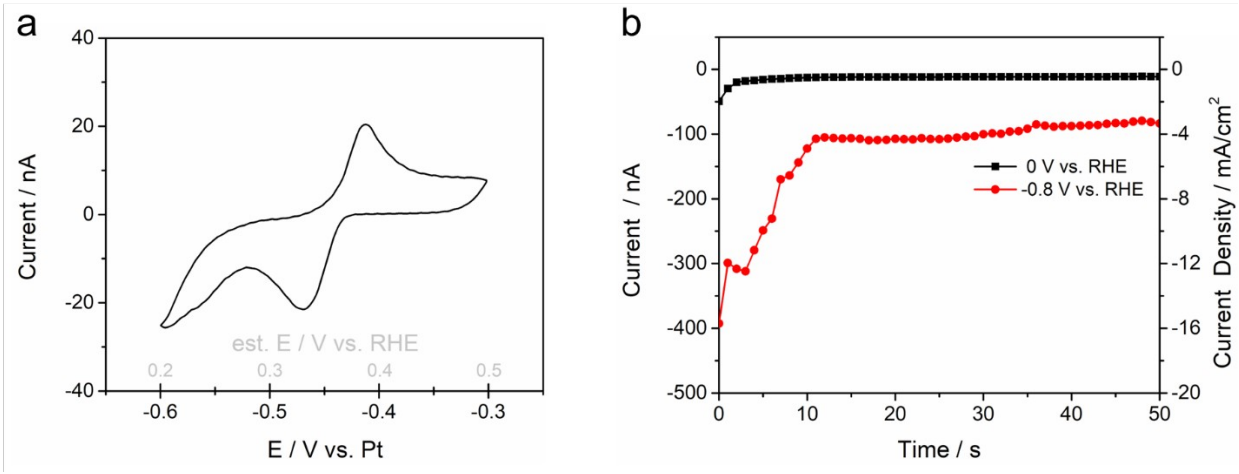

Figure 2. (a) CV profile of a 7 nm Cu NP ensemble on the carbon WE in CO_2-saturated 0.1 M $KHCO_3$ at 100 mV/s. (b) Corresponding CA profiles at 0 and -0.8 V vs. RHE with current and current density as the left and right Y-axes, respectively.

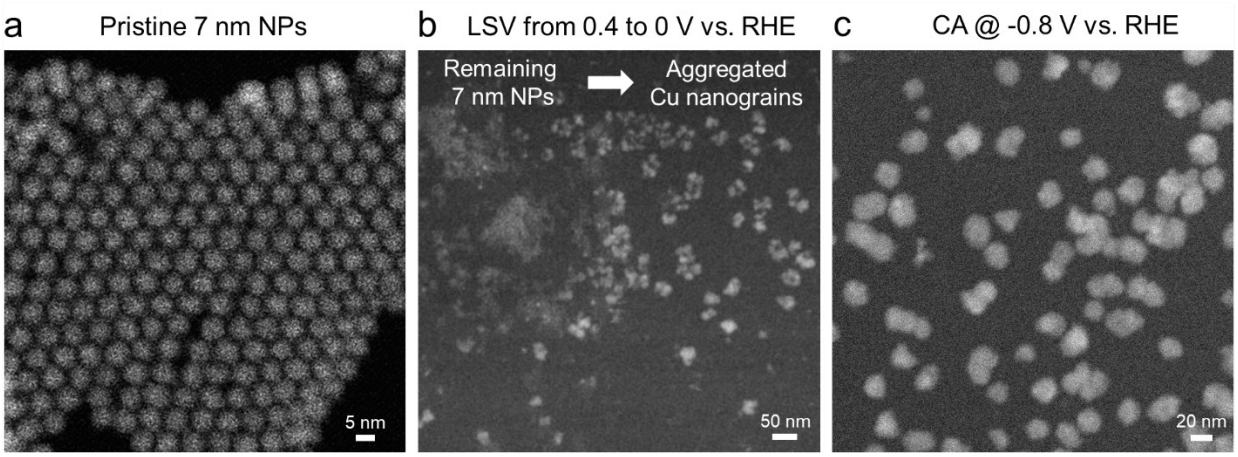

Figure 3. Dynamic evolution of the 7 nm NP ensemble under CO_2RR-relevant conditions. (a) HAADF-STEM image of monolayer NP ensemble. (b) *Operando* EC-STEM images capturing both the remaining 7 nm NPs and the initial formation of loosely connected Cu nanograins after LSV scan from 0.4 to 0 V vs. RHE. (c) *Operando* EC-STEM image of the steady-state formation of closely packed Cu nanograins after CA at -0.8 V vs. RHE.

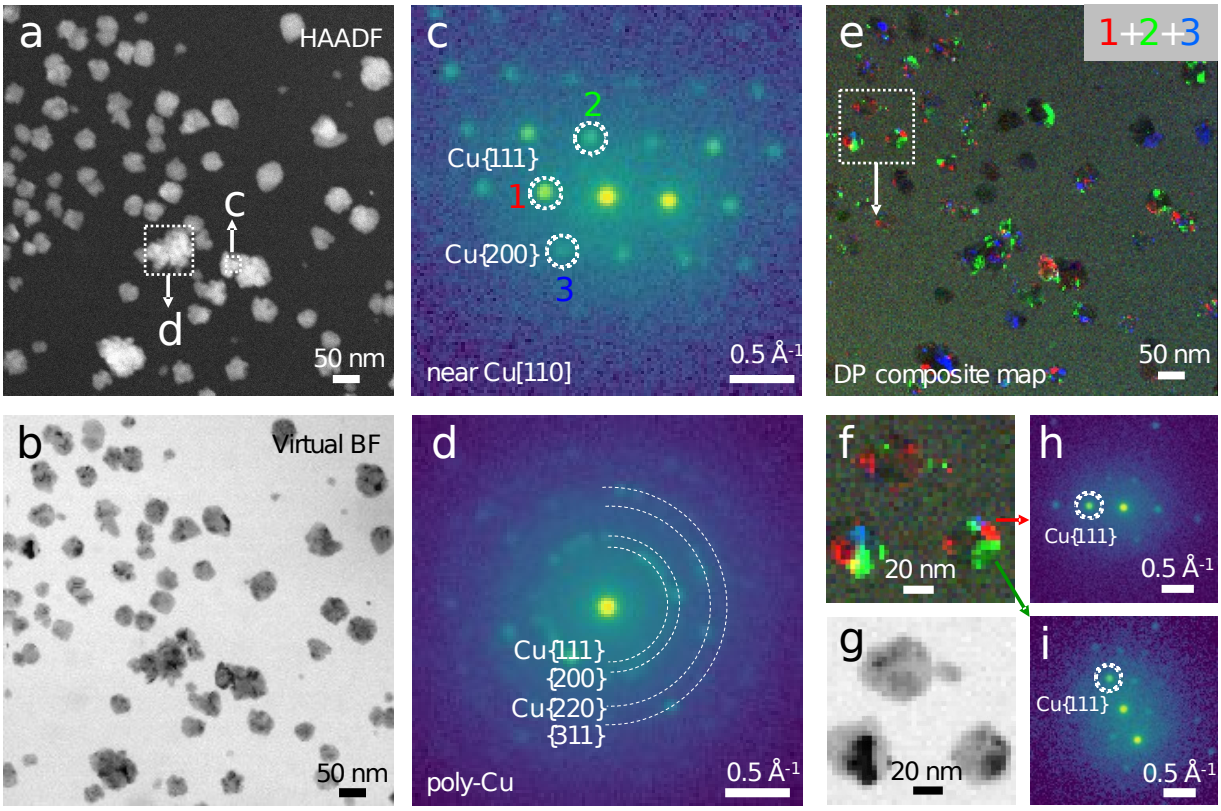

Figure 4. *Operando* electrochemical 4D-STEM diffraction imaging of Cu nanograins generated at -0.8 V vs. RHE. (a-b) HAADF-STEM image and corresponding virtual BF-STEM image extracted from the central disk in the 4D-STEM dataset. (c-d) Representative diffraction patterns near the Cu[110] zone axis and polycrystalline Cu of Cu nanograins labeled in (a). (e) False-color dark-field 4D-STEM composite images showing polycrystalline Cu nanograins extracted from diffraction spots marked as 1 (red), 2 (green) and 3 (blue), respectively, in (c). (f-g) Magnified region from the dashed box in (e) and (g) corresponding virtual BF-STEM image. (h-l) Diffraction patterns corresponding to Cu domains 1 (red) and 2 (green) in (f), respectively.

Supporting Information:
Experimental methods (NP synthesis, *operando* EC-STEM and 4D-STEM measurements); Figures S1-S5 and Table S1, additional electrochemical, EC-STEM and EELS measurements.

Corresponding Authors:
Y.Y.: yaoyang1@berkeley.edu
H.D.A.: hda1@cornell.edu
P.Y.: p_yang@berkeley.edu

Acknowledgement:
This work was supported by Director, Office of Science, Office of Basic Energy Sciences, Chemical Sciences, Geosciences, & Biosciences Division, of the US Department of Energy under Contract DE-AC02-05CH11231, FWP CH030201 (Catalysis Research Program). *Operando* EC-STEM was supported by the Center for Alkaline-Based Energy Solutions

(CABES), an Energy Frontier Research Center (EFRC) program supported by the U.S. Department of Energy, under grant DE-SC0019445. This work made use of TEM facilities at the CCMR which are supported through the National Science Foundation Materials Research Science and Engineering Center (NSF MRSEC) program (DMR-1719875). This work also used TEM facilities at the Molecular Foundry was supported by the Office of Science, Office of Basic Energy Sciences, of the U.S. Department of Energy under Contract No. DE-AC02-05CH11231. Y.Y. acknowledges the support from the Miller Research Fellowship. J.J. and C.C. acknowledge the support from Suzhou Industrial Park Scholarship. S.Y. acknowledges support from Samsung Scholarship. We dedicate this work to Prof. Héctor Abruña's 70th birthday and over 40-years of contributions to *Operando* Electrochemistry.

Competing interests:

The authors declare no competing financial interest.

References.

1. Yang, Y.; Louisia, S.; Yu, S.; Jin, J.; Roh, I.; Chen, C.; Fonseca Guzman, M. V.; Feijoo, J.; Chen, P.; Wang, H.; Pollock, C. J.; Huang, X.; Shao, Y.-T.; Wang, C. Muller, D. A.; Abruña, H. D.; Yang, P. *Operando* Studies Reveal Active Cu Nanograins for CO_2 Electroreduction. *Nature* **2022**, DOI:10.1038/s41586-022-05540-0.
2. Abruña, H. D.; Bommarito, G. M.; Acevedo, D. The Study of Solid/Liquid Interfaces with X-ray Standing Waves. *Science* **1990**, 250, 69-74.
3. Abruña, H. D. Electrochemical Interface: Modern Techniques for In Situ Interface Characterization VCH: New York, **1991**.
4. Yang, Y..; Xiong, Y.; Zeng, R.; Lu, X.; Krumov, M.; Huang, X.; Xu, W.; Wang, H.; DiSalvo, F. J.; Brock, J. D.; Muller, D. A.; Abruña, H. D. *Operando* Methods in Electrocatalysis. *ACS Catal*. **2021**, *11*, 1136-1178.
5. Weckhuysen, B. M. Snapshots of a Working Catalyst: Possibilities and Limitations of *In Situ* Spectroscopy in the Field of Heterogeneous Catalysis. *Chem. Commun*. **2002**, 97-110.
6. Bañares, M. A. *Operando* Methodology: Combination of In Situ Spectroscopy and Simultaneous Activity Measurements under Catalytic Reaction Conditions. *Catal. Today* **2005**, *100*, 71-77.
7. Williamson, M.; Tromp, R.; Vereecken, P.; Hull, R.; Ross, F. Dynamic Microscopy of Nanoscale Cluster Growth at the Solid–Liquid Interface. *Nat. Mater*. **2003**, *2*, 532-536.
8. Li, Y.; Kim, D.; Louisia, S.; Xie, C.; Kong, Q.; Yu, S.; Lin, T.; Aloni, S.; Fakra, S.; Yang, P. Electrochemically scrambled nanocrystals are catalytically active for CO_2-tomulticarbons. *Proc. Natl. Acad. Sci. USA* **2020**, *117,* 9194-9201.
9. Kim, D.; Kley, C. S.; Li, Y.; Yang, P. Copper Nanoparticle Ensembles for Selective Electroreduction of CO_2 to C_2–C_3 products. *Proc. Natl. Acad. Sci. USA* **2017**, *114*, 10560-10565.
10. Holtz, M. E.; Yu, Y.; Gao, J.; Abruña, H. D.; Muller D. A. *In Situ* Electron Energy-Loss Spectroscopy in Liquids. *Microsc. Microanal*. **2013**, *19*, 1027-1035.
11. de Jonge, N.; Houben, L.; Dunin-Borkowski, R. E.; Ross, F. M. Resolution and Aberration Correction in Liquid Cell Transmission Electron Microscopy. *Nat. Rev. Mater*. **2019**, *4*, 61-78.
12. Khelfa, A.; Byun, C.; Nelayah, J.; Wang, G.; Ricolleau, C.; Alloyeau, D. Structural Analysis of Single NPs In Liquid by Low-Dose STEM Nanodiffraction. *Micron* **2019**, *116*, 30-35.
13. Karakulina, O. M.; Demortiere, A.; Dachraoui, W.; Abakumov, A. M.; Hadermann, J. In Situ Electron Diffraction Tomography Using A Liquid-Electrochemical Transmission Electron Microscopy Cell for Crystal Structure Determination of Cathode Materials for Li-Ion Batteries. *Nano Lett*. **2018**, *18*, 6286-6291.
14. Serra-Maia, R.; Kumar, P.; Meng, A. C.; Foucher, A. C.; Kang, Y.; Karki, K.; Jariwala, D.; Stach, E. A. Nanoscale Chemical and Structural Analysis during In Situ Scanning/Transmission Electron Microscopy in Liquids. *ACS Nano* **2021**, *15*, 10228-10240.

15. Yang, Y.; Shao, Y.-T.; Lu, X.; Yang, Y.; Ko, H.-Y.; DiStasio, R. A.; DiSalvo, F. J.; Muller, D. A.; Abruña, H. D. *J. Am. Chem. Soc*. **2022**, 144, 15698-15708.
16. Holtz, M. E.; Yu, Y.; Gunceler, D.; Gao, J.; Sundararaman, R.; Schwarz, K. A.; Arias, T. A.; Abruña, H. D.; Muller D. A. Nanoscale Imaging of Lithium Ion Distribution during *In Situ* Operation of Battery Electrode and Electrolyte. *Nano Lett*. **2014**, 14, 1453-1459.
17. Yang, Y.; Shao, Y.-T.; Lu, X.; Abruña, H. D.; Muller, D. A. Metal Monolayers on Command: Underpotential Deposition at Nanocrystal Surfaces: A Quantitative *Operando* Electrochemical Transmission Electron Microscopy Study. *ACS Energy Lett.* **2022**, *7*, 1292-1297.
18. Egerton, R. F.; Cheng, S. C. Measurement of Local Thickness by Electron Energy-Loss Spectroscopy. *Ultramicroscopy* **1987**, 21, 231-244.
19. Yang, Y.; Roh, I.; Louisia, S.; Yu, S.; Chen, C.; Jin, J.; Yu, S.; Salmeron, M. B.; Wang, C.; Yang, P. *Operando* Resonant Soft X-ray Scattering Studies of Chemical Environment and Interparticle Dynamics of Cu Nanocatalysts for CO_2 Electroreduction. ***J. Am. Chem. Soc***. 2022, *144*, 8927-8931.
20. Tate, M. W.; Purohit, P.; Chamberlain, D.; Nguyen, K. X.; Hovden, R.; Chang, C. S.; Deb, P.; Turgut, E.; Heron, J. T.; Schlom, D. G.; Ralph, D.; Fuchs, G. D.; Shanks, K. S.; Philipp, H. T.; Muller, D. A.; Gruner, S. M. High Dynamic Range Pixel Array Detector for Scanning Transmission Electron Microscopy. *Microsc. Microanal*. **2016**, *22*, 237-249.
21. Chen, Z.; Jiang, Y.; Shao, Y.-T.; Holtz, M. E.; Odstrcil, M.; Guizar-Sicairos, M.; Hanke, I.; Ganschow, S.; Schlom, D. G.; Muller, D. A. Electron Ptychorgraphy Achieves Atomic-Resolution Limits Set by Lattice Vibrations. *Science* **2021**, *372*, 826-831.
22. Feng, L. et al. Interplay of Electrochemical and Electrical Effects Induces Structural Transformations in Electrocatalysts. *Nat. Catal*. **2021**, *4*, 479-487.
23. Sun, K.; Yu, K.; Fang, J.; Zhuang, Z.; Tan, X.; Wu, Y.; Zeng, L.; Zhuang, Z.; Pan, Y.; Chen, C. Nature-Inspired Design of Molybdenum–Selenium Dual-Single-Atom Electrocatalysts for CO_2 Reduction. *Adv. Mater.* **2022,** *34*, 2206478.
24. Liu, C.; Wu, Y.; Sun, K.; Fang, J.; Huang, A.; Pan, Y.; Cheong, W.-C.; Zhuang, Z.; Zhuang, Z.; Yuan, Q.; Xin, H. L.; Zhang, C.; Zhang, J.; Xiao, H.; Chen, C.; Li, Y. Constructing FeN_4/graphitic Nitrogen Atomic Interface for High-Efficiency Electrochemical CO_2 Reduction over a Broad Potential Window. *Chem* **2021**, *7*, 1297-1307.
25. Grosse, P.; Yoon, A.; Rettenmaier, C.; Herzog, A.; Chee, S. W.; Roldan Cuenya, B. Dynamic Transformation of Cubic Copper Catalysts during CO_2 Electroreduction and its Impact on Catalytic Selectivity. *Nat. Commun*. **2021**, 12, 6736.
26. Walker, N. L.; Dick, J. E. Leakless, Bipolar Reference Electrode: Fabrication, Performance and Miniaturization. *Anal. Chem*. **2021**, *93*, 10065-10074.
27. Unocic, R. R.; Sacci, R. L.; Brown, G. M.; Veith, G. M.; Dudney, N. J.; More, K. M.; Walden II, F. S.; Gardiner, D. S.; Damiano, J.; Nackashi, D. P. Quantitative electrochemical measurements using in situ EC-S/TEM devices. *Microsc. Microanal*. **2014**, *20*, 452-461.
28. Yang, Y. *et al.* Electrocatalysis in Alkaline Media and Alkaline Membrane-Based Energy Technologies. *Chem. Rev*. **2022**, *122*, 6117-6321.
29. Beermann, V.; Holtz, M. E.; Padgett, E.; de Araujo, J. F.; Muller, D. A.; Strasser, P. Real-Time Imaging of Activation and Degradation of Carbon Supported Octahedral Pt–Ni Alloy Fuel Cell Catalysts at the Nanoscale Using In Situ Electrochemical Liquid Cell STEM. *Energy. Envion. Sci.* **2019**, *12*, 2476-2485.
30. Sacci, R. L.; Black, J. M.; Balke, N.; Dudney, N. J.; More, K. L.; Unocic, R. R. Nanoscale Imaging of Fundamental Li Battery Chemistry: Solid-Electrolyte Interphase Formation and Preferential Growth of Lithium Metal Nanoclusters. *Nano Lett.* **2015**, *15*, 2011-2018.

For Table of Content Use Only

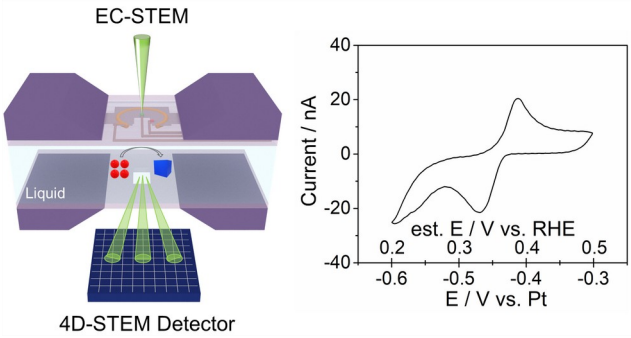

Operando EC-STEM enables quantitative electrochemistry and simultaneously probes time-resolved structural changes of sub-10 nm Cu nanocatalysts for sustainable CO_2 electroreduction.